Journal of Geophysical Research: Atmospheres

Supporting Information for

Contribution of the Southern Annular Mode to variations in water isotopes of daily precipitation at Dome Fuji, East Antarctica

K. Kino[1,2], A. Okazaki[3], A. Cauquoin[2], and K. Yoshimura[2]

[1]Atmosphere and Ocean Research Institute, The University of Tokyo, Kashiwa, Japan

[2]Institute of Industrial Science, The University of Tokyo, Kashiwa, Japan

[3]Hirosaki University, Hirosaki, Japan

Contents of this file

Introduction

This supporting information provides the following:

(i) Text S1 and Figure S7:

The possible causes of the model-data discrepancy for two precipitation events in austral summer (Figure 2c) are investigated.

(ii) Figure S1:

Different datasets, including isotopic measurements in precipitation, ice cores, and continental speleothems, were used as in Cauquoin et al. (2019b) and compared with the simulation results for global evaluation (Figure S1). The observed $\delta^{18}O_p$ values were obtained from the Global Network for Isotopes in Precipitation (GNIP) observational database for at least five calendar years from 1961 to 2007 (IAEA/WMO, 2018). The ice core data are presented in Table 1 of Cauquoin et al. (2019). $\delta^{18}O$ in the calcite of speleothem was obtained from the Speleothem Isotope Synthesis and Analysis (SISAL) dataset (version 1b: Atsawawaranunt et al., 2019) updated by Comas-Bru et al. (2019). The speleothem values of $\delta^{18}O$ in calcite are converted to $\delta^{18}O$ in drip water as in Cauquoin et al. (2019b) using ERA-40 reanalysis data (Kållberg et al., 2004) and method of Tremaine et al. (2011). The simulated $\delta^{18}O_p$ was in good agreement with present-day observations (Figure S1). The known features of the isotopic effects found by Dansgaard (1964) were well simulated, as confirmed by Okazaki & Yoshimura (2019), namely, enhanced depletion with latitude, altitude, and continentality.

(iii) Figures S2 to S4:

Simulated daily SAT, precipitation, and $\delta^{18}O_p$ were evaluated by comparing the results with the observations of Stenni et al. (2016) in EPICA Dome C from 2008 to 2010.

(iv) Figure S5:

The monthly climatologies of simulated SAT and $\delta^{18}O_p$ at Dome Fuji, with and without weighting by precipitation amount.

(v) Figure S6:

The annual and JJA mean climatologies for simulated vertically integrated $\delta^{18}O_v$ and simulated meridional moisture flux.

(vi) Tables S1 and S2:

Statistical analyses for the simulation results (Table S1) and in-situ observation results at Dome Fuji (Fujita and Abe, 2006; Table S2) were conducted. We used the absolute values because we could not determine the climatology of the observation.

(vii) Table S3:

Same as Table S1 for the entire period of 1981–2010. For SAT and $\delta^{18}O_p$, we used the deviations as described in Section 2.4.

(viii) Table S4:

Standard deviations of modeled daily SAT and $\delta^{18}O_p$ in each month for the entire period of 1981–2010 are also shown in Figure 3.

Text S1.

The precipitation event at the beginning of December 2003 was induced by air intrusion between the ridge and the trough on the continent and the Atlantic ocean, respectively (Figure S7a). Then, the radiative cooling with high pressure expanded toward Dome Fuji (Figure S7b). The moisture inflow around Dome Fuji gave relatively large precipitation with decreasing SAT and $\delta^{18}O_p$ until 4 December (Figure 1), similar to a typical precipitation event during the austral winter. After that day, SAT increased while $\delta^{18}O_p$ was decreasing (Figure 1), suggesting the radiative cooling induced precipitation, and the "precipitation effect" was dominant for $\delta^{18}O_p$. However, only the second half of the simulated feature was confirmed in observation (Figure 1). The low model resolution may induce model-data discrepancies. If the high pressure had expanded toward Dome Fuji before 4 December, it would reduce the overestimation of inflow and accompanying precipitation there.

The overestimation of inflow might also cause the overestimated precipitation event at the beginning of January 2004. The southerly flow-induced this simulated precipitation event (Figure S7c), and the air mass passed over Antarctica then reached Dome Fuji. Because the decreasing trends in simulated SAT and $\delta^{18}O_p$ were comparable to those in observation, the model was supposed to reproduce the dynamical circulation reasonably but may overestimate inflows again.

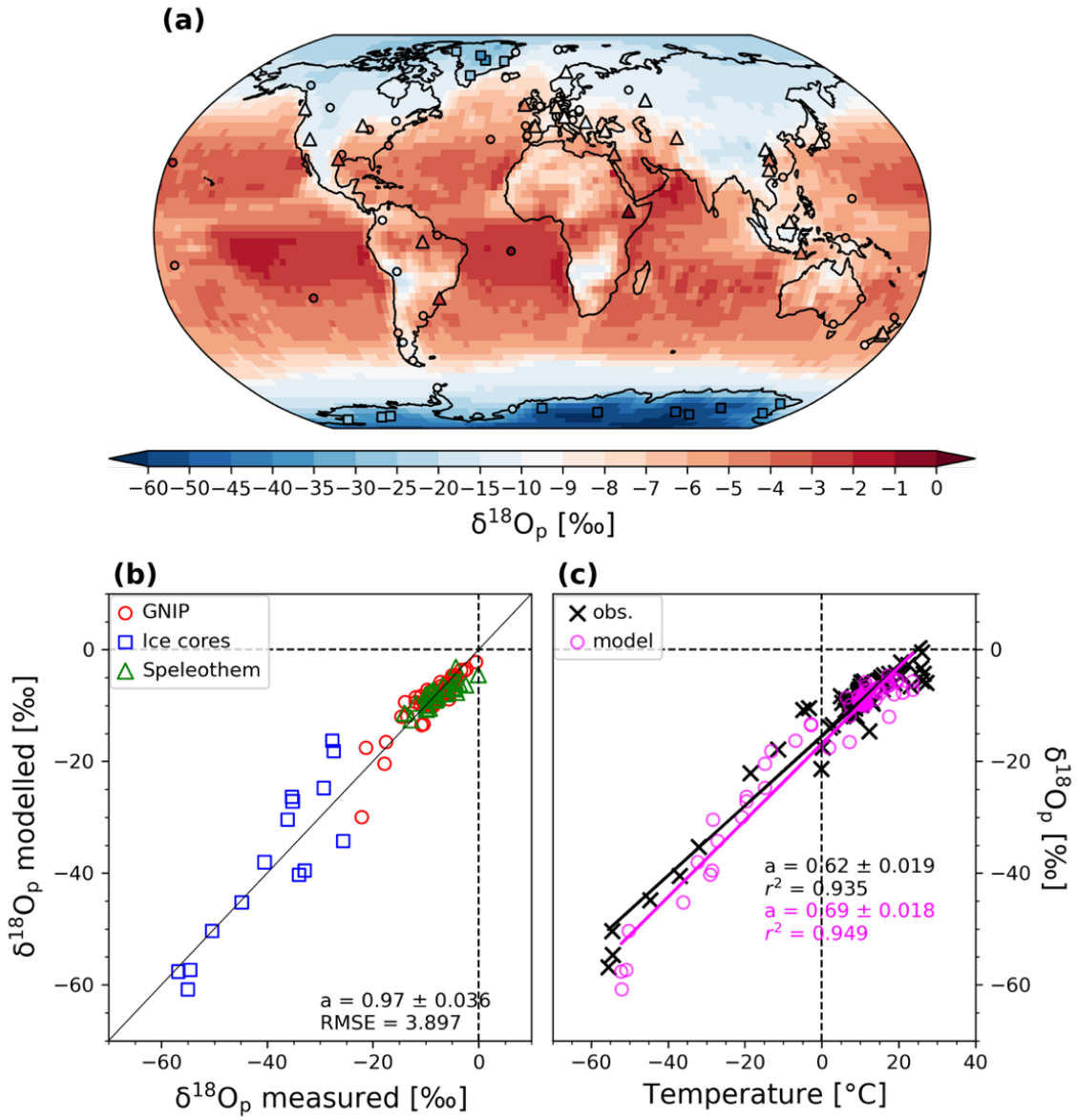

Figure S1. (**a)** Global climatological distribution of simulated (background pattern) and observed (colored markers; see text for details) annual mean $\delta^{18}O$ values in precipitation. The data consist of 70 GNIP stations (circles), 15 ice core records (squares), and 33 speleothem records (triangles). **(b)** Modeled vs. observed annual mean $\delta^{18}O_p$ at the different GNIP, speleothem, and ice core sites. **(c)** Observed (black crosses) and modeled (magenta circles) spatial $\delta^{18}O_p$–surface air temperature relationship. The linear fits for the observed and modeled values are drawn as black and magenta lines, respectively. For **(b)** and **(c)**, the gradients of the linear regression fits are expressed in each panel.

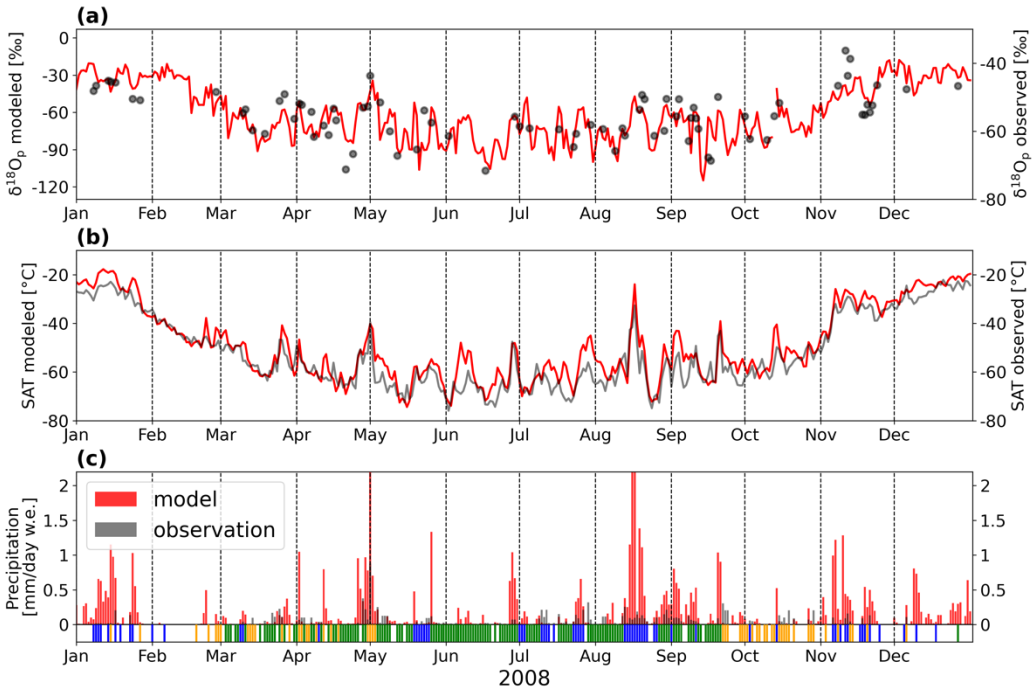

Figure S2. (a) Seasonal changes in simulated (red; left y-axes) and observed (black; right y-axes; Stenni et al., 2016) **(a)** $\delta^{18}O_p$, **(b)** surface air temperature, and **(c)** daily mean precipitation in water equivalent at Dome C for the year 2008. For **(c)**, types of observed precipitation of each day are also shown in the bottom as colored bars: snowfall (yellow), hoar frost (green), diamond dust (blue), and no observation (white).

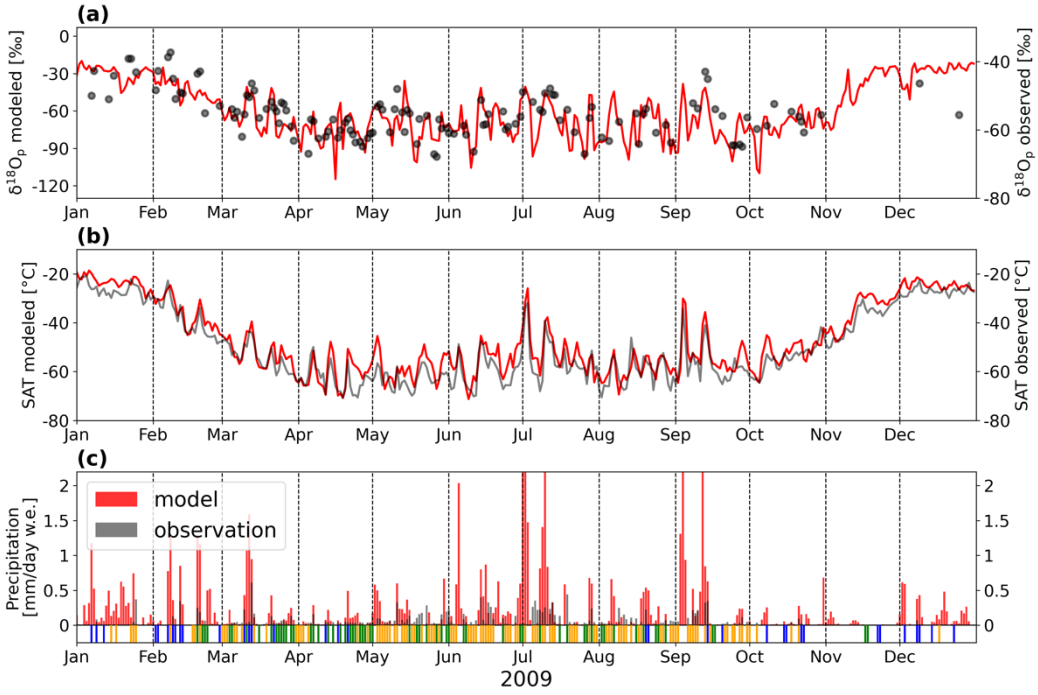

Figure S3. Same as Figure S2 but for 2009.

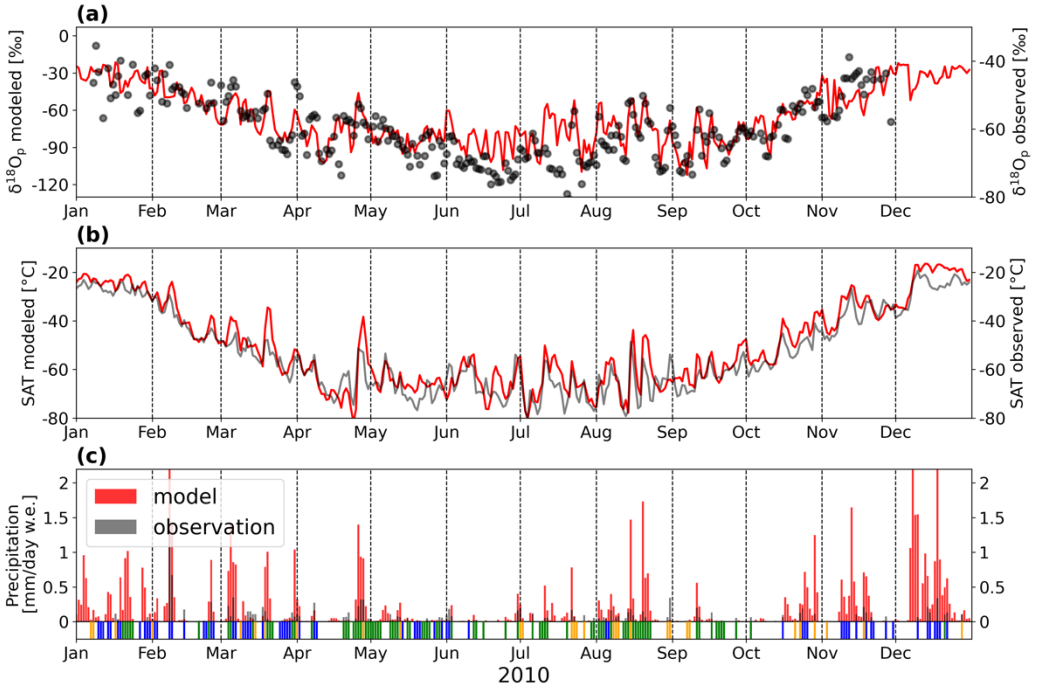

Figure S4. Same as Figure S2 but for 2010.

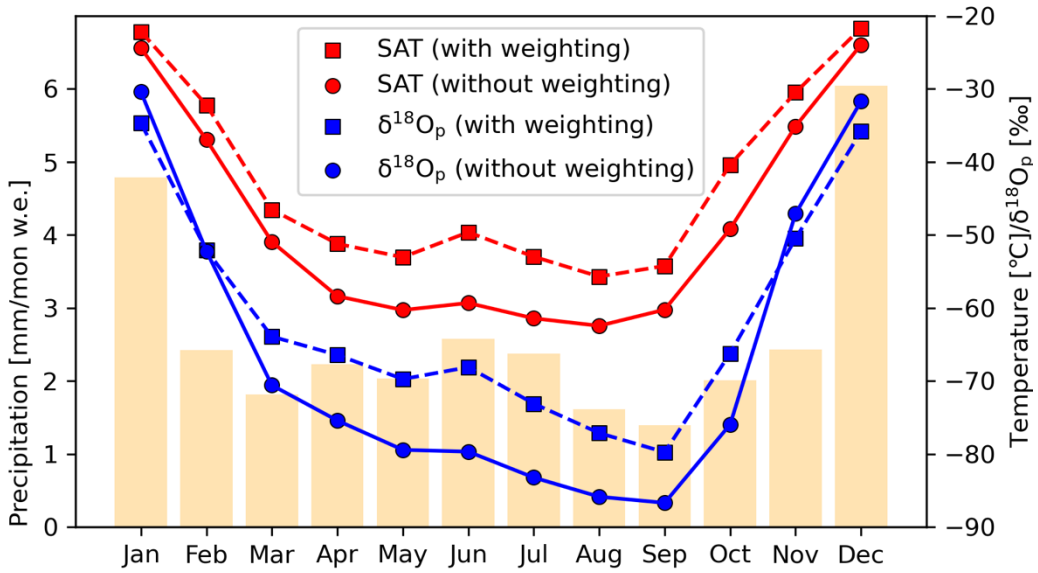

Figure S5. Simulated precipitation (bars; left y-axis), SAT (red; right y-axis), and $\delta^{18}O_p$ (blue; right y-axis) of monthly climatologies. For SAT and $\delta^{18}O_p$, both with and without weighting by precipitation amount are shown by squares with dashed lines and circles with solid lines, respectively. Again, in the legend SAT (with weighting), SAT (no weighting), $\delta^{18}O_p$ (with weighting), $\delta^{18}O_p$ (no weighting).

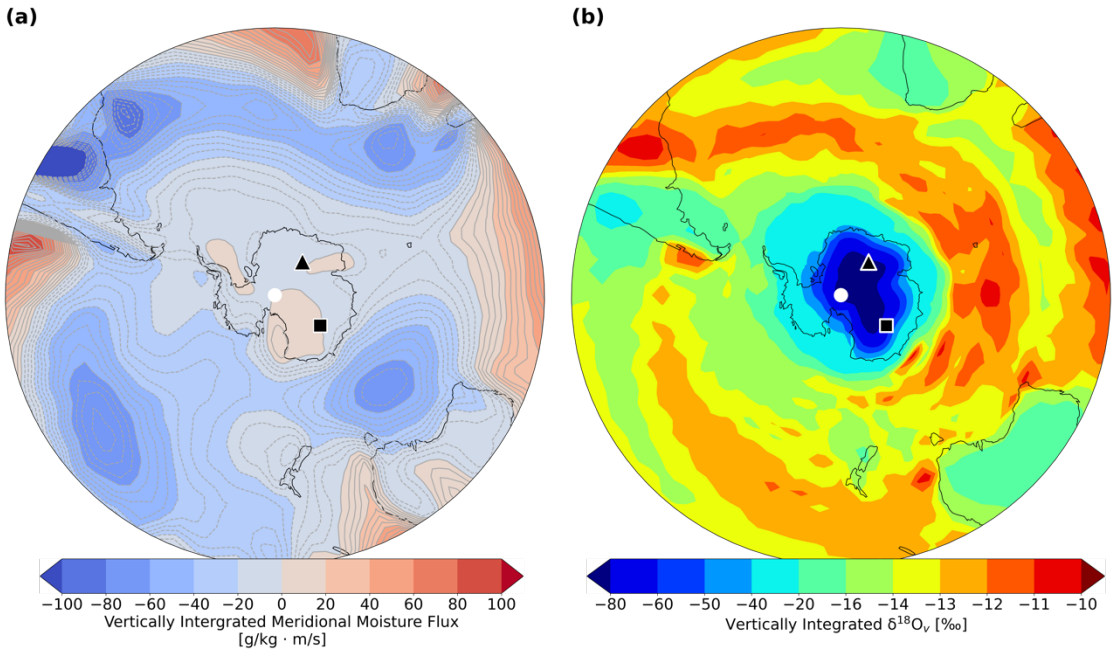

Figure S6. Simulated climatologies in JJA for **(a)** meridional moisture flux and **(b)** vertically integrated $\delta^{18}O_v$. For **(a)**, contours are supplementarily drawn in every 5 g/kg•m/s; northward flux in solid lines; and southward flux in dashed lines. For **(a)** and **(b)**, the location of Dome Fuji and Dome C is plotted as a triangle and square, respectively.

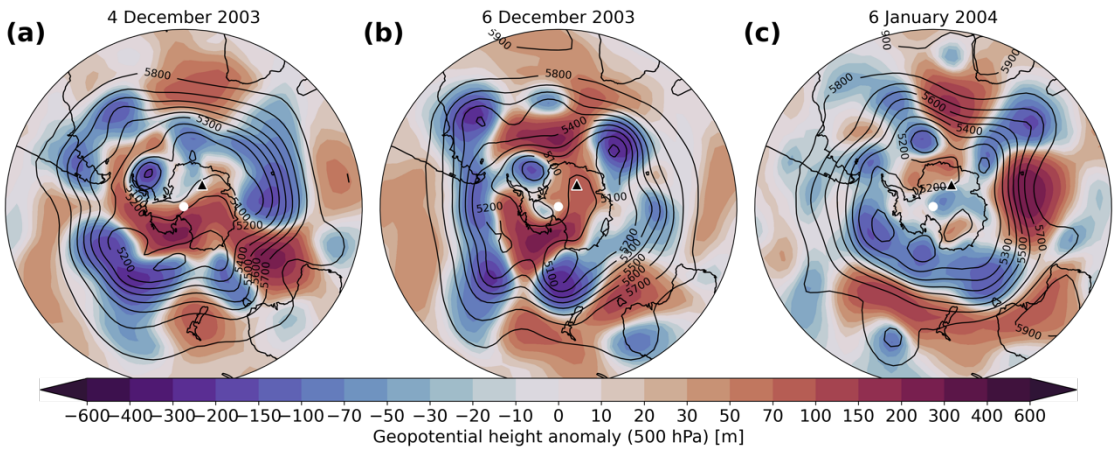

Figure S7. Simulated geopotential height (contours) and its deviation from daily climatology (colors) on **(a)** 4 December 2003; **(b)** 6 December 2003; and **(c)** 6 January 2004. For **(a**–**c)**, the location of Dome Fuji is plotted as a triangle.

	Jan	Feb	Mar	Apr	May	Jun	Jul	Aug	Sep	Oct	Nov	Dec
Number of days	18	23	31	29	31	30	29	31	29	25	26	26
R_{SAT}	NaN	NaN	0.63	0.50	NaN	NaN	0.36	0.57	0.36	0.38	0.37	NaN
p_{SAT}	8.80E-01	9.96E-01	1.54E-04	5.97E-03	7.94E-01	1.04E-01	5.57E-02	8.21E-04	5.39E-02	5.82E-02	6.42E-02	5.96E-01
R_{Pr}	-0.74	NaN	0.50	0.52	NaN	0.58	0.43	0.75	0.41	NaN	NaN	-0.51
p_{Pr}	4.47E-04	5.11E-01	4.08E-03	3.78E-03	6.43E-01	7.72E-04	1.99E-02	1.43E-06	2.70E-02	6.63E-01	1.40E-01	8.11E-03
R_{SAM}	-0.44	0.47	-0.32	0.34	NaN	NaN	-0.60	NaN	NaN	NaN	NaN	NaN
p_{SAM}	6.44E-02	2.32E-02	8.07E-02	7.52E-02	5.98E-01	1.57E-01	6.12E-04	7.40E-01	2.63E-01	5.24E-01	2.71E-01	4.20E-01

Table S1. Spearman's correlation coefficients and p-values between modeled daily $\delta^{18}O_p$, and surface air temperature (R_{SAT} and p_{SAT}), precipitation (R_{Pr} and p_{Pr}), and SAM index (R_{SAM} and p_{SAM}) in each month for the period of the observation (from 3 February 2003 to 20 January 2004). Only correlation coefficients with p-values lower than 0.1 are shown (NaN if not). Only the days with valid values in the simulation and the observation (shown in Table S2) were analyzed. The number of effective days was shown for respective months.

	Jan	Feb	Mar	Apr	May	Jun	Jul	Aug	Sep	Oct	Nov	Dec
Number of days	18	23	31	29	31	30	29	31	29	25	26	26
R_{SAT}	0.65	0.56	0.47	0.40	NaN	0.46	0.60	0.57	0.44	0.51	0.82	0.37
p_{SAT}	3.70E-03	5.94E-03	7.15E-03	3.13E-02	7.66E-01	1.02E-02	5.29E-04	8.83E-04	1.72E-02	9.83E-03	2.92E-07	6.26E-02
R_{Pr}	NaN	NaN	NaN	0.43	0.59	0.77	0.73	0.59	0.46	NaN	0.34	NaN
p_{Pr}	5.02E-01	1.05E-01	5.97E-01	1.97E-02	4.91E-04	5.29E-07	7.17E-06	5.10E-04	1.26E-02	1.30E-01	9.02E-02	3.44E-01
R_{SAM}	NaN	0.39	-0.57	NaN	NaN	NaN	NaN	NaN	-0.51	NaN	-0.57	NaN
p_{SAM}	2.91E-01	6.71E-02	7.54E-04	5.62E-01	6.48E-01	1.26E-01	1.03E-01	1.64E-01	4.82E-03	9.80E-01	2.17E-03	1.35E-01

Table S2. Same as Table S1 but for observation at Dome Fuji (Fujita and Abe, 2006) and the Japanese 25-year reanalysis fields (Onogi et al., 2007).

	Jan	Feb	Mar	Apr	May	Jun	Jul	Aug	Sep	Oct	Nov	Dec
Number of days	930	847	930	900	930	900	930	930	896	858	893	930
R_{SAT}	-0.27	0.15	0.44	0.41	0.45	0.54	0.54	0.48	0.43	0.44	NaN	-0.18
p_{SAT}	9.31E-17	8.60E-06	1.36E-44	7.50E-37	1.17E-47	1.15E-69	1.30E-72	4.35E-55	1.20E-41	1.18E-42	8.53E-02	1.45E-08
R_{Pr}	-0.52	-0.18	0.43	0.56	0.46	0.49	0.46	0.42	0.46	0.29	-0.37	-0.55
p_{Pr}	3.48E-64	8.81E-08	1.31E-42	3.99E-76	5.10E-51	2.25E-56	9.22E-51	1.10E-41	8.14E-49	1.52E-18	1.17E-29	4.56E-75
R_{SAM}	NaN	-0.11	-0.18	-0.16	-0.28	-0.35	-0.49	-0.39	-0.33	-0.34	-0.24	-0.10
p_{SAM}	8.85E-02	9.43E-04	7.20E-08	1.43E-06	1.30E-17	4.23E-28	1.91E-57	4.91E-36	4.71E-24	1.74E-25	1.23E-13	2.05E-03

Table S3. Spearman's correlation coefficients and p-values between modeled daily $\delta^{18}O_p$ and SAT (R_{SAT} and p_{SAT}), precipitation (R_{Pr} and p_{Pr}), and SAM index (R_{SAM} and p_{SAM}) in each month. For $\delta^{18}O_p$ and SAT, deviations from daily climatology for the entire period of 1981–2010 were used, as described in Section 2.4. Only correlation coefficients with p-values lower than 0.05 are shown (NaN if not). The number of effective days used for the analysis was also shown for respective months.

	Jan	Feb	Mar	Apr	May	Jun	Jul	Aug	Sep	Oct	Nov	Dec
SAT [°C]	2.77	4.49	5.72	6.86	8.24	8.45	8.57	7.41	6.97	6.21	4.51	2.77
$\delta^{18}O_p$ [‰]	6.62	8.34	9.28	10.50	12.29	12.18	13.33	12.31	12.25	13.57	9.47	6.82

Table S4. Standard deviations of modeled daily SAT and $\delta^{18}O_p$ in each month. Deviations from daily climatology for the entire period of 1981–2010 were used for each variable, as described in Section 2.4.